Laetirobin from the Parasitic Growth of Laetiporus sulphureus on Robinia pseudoacacia

ARTICLE *in* JOURNAL OF NATURAL PRODUCTS · OCTOBER 2009

Impact Factor: 3.8 · DOI: 10.1021/np9002838 · Source: PubMed

Laetirobin from the Parasitic Growth of *Laetiporus sulphureus* on *Robinia pseudoacacia*

Martin J. Lear,*[,†] Oliver Simon,[†] Timothy L. Foley,[‡] Michael D. Burkart,[‡] Thomas J. Baiga,[§] Joseph P. Noel,[§] Antonio G. DiPasquale,[‡] Arnold L. Rheingold,[‡] and James J. La Clair*[,∞]

Department of Chemistry, and Medicinal Chemistry Program of the Life Sciences Institute, National University of Singapore, 3 Science Drive 3, Singapore 117543, Department of Chemistry and Biochemistry, University of California, San Diego, 9500 Gilman Drive, La Jolla, California 92093, Howard Hughes Medical Institute, Jack H. Skirball Center for Chemical Biology and Proteomics, The Salk Institute for Biological Studies, La Jolla, California 92037, and Xenobe Research Institute, 3371 Adams Avenue, San Diego, California 92116

Received May 8, 2009

(±)-Laetirobin (**1**) was isolated as a cytostatic lead from *Laetiporus sulphureus* growing parasitically on the black locust tree, *Robinia pseudoacacia*, by virtue of a reverse-immunoaffinity system. Using an LC/MS procedure, milligram quantities of (±)-laetirobin (**1**) were obtained, and the structure of **1** was elucidated by X-ray crystallography and confirmed by NMR spectroscopy. Preliminary cellular studies indicated that (±)-laetirobin (**1**) rapidly enters in tumor cells, blocks cell division at a late stage of mitosis, and invokes apoptosis.

Natural products continue to offer unique opportunities in drug discovery by harnessing new structural information with inbuilt biological activity.[1] Ongoing challenges are to select unique sources of natural product leads and develop expedient biological screening methods. Among such strategies,[2] the discovery of unforeseen biological leads is often enhanced by studying the way ecological and environmental variables regulate the production of secondary metabolites.[3] In this study, we targeted agents that could disrupt tumor cell division and elected to screen for metabolites that were produced at the intersection of plants and polypore fungi.[4] Our studies soon led to *Laetiporus sulphureus*,[5] a species known to display toxicity when growing parasitically on the black locust tree, *Robinia pseudoacacia*.[6] We selected a reverse-affinity approach for our screening strategy.[7a] Combining this system with fluorescent labeling[8] (to increase the sensitivity of the method), we isolated and characterized (±)-laetirobin (**1**). Preliminary biological studies indicate that (±)-laetirobin (**1**) offers a robust cytostatic activity.

Results and Discussion

Specimens of *L. sulphureus* were collected from parasitic and saprobic environments from three plant hosts, *R. pseudoacacia*, *Eucalyptus cladocalyx*, and *Quercus dumosa*. A total of seven crude extracts were prepared (step a, Figure 1) and screened for activity against human cervical cancer (HeLa), human colon carcinoma (HCT116), and mouse neuroblastoma (Neuro-2a) cell lines. Only the two extracts obtained from the parasitic pairing of *L. sulphureus* with *R. pseudoacacia* (specimens XRI2009 and XRI2132) displayed cytostatic effects at ≤100 μg/mL. This suggested a parasitic response between the fungus and plant. In order to further characterize the phenotype, we evaluated the effects of each extract on the cell cycle using a fluorescent staining protocol.[9] In three cell lines, we observed a uniform blockage of cells treated with the active extracts during G2−S stages during mitosis (HeLa, IC_{50} values of 1.2 ± 0.2 and 3.2 ± 0.1 μg/mL; HCT116, IC_{50} values of 3.5 ± 0.2 and 9.1 ± 0.3 μg/mL; Neuro-2a, IC_{50} values of 0.82 ± 0.21 and 0.67 ± 0.12 μg/mL). We then repeated the procedure using synchronized cells.[10] Exposure during G1, S, or G2, or prior to entering mitosis (M) led to a comparable block during mitosis, although treatment at G2 or prior to M gave enhanced effects.

Having identified active crude extracts from parasitic *Laetiporus* specimens, we began to screen for natural components with inherent affinity to the proteome of human tumor cells; the idea being that compounds delivering a potent mitotic activity would likely bind to proteins within tumor cell lysates. To this end, we tailored a reverse-affinity system[7a] to hold five resin-bound protein columns from different subcellular fractions of lysed HeLa cells (Figure 1). Each resin was used to capture natural product material (step b, Figure 1). This provided fractions **A1**−**A5** enriched with compounds that could bind to HeLa expressed proteins (step c, Figure 1). Treatment of fractions **A1**−**A5** with the immunoaffinity fluorescent (IAF) label aziridine **2**[8] provided fractions **B1**−**B5** containing IAF-labeled compounds (step d, Figure 1). A fluorescent labeling step was used to improve the detection limit of the method as well as to enable a subsequent affinity purification step. The IAF-labeled materials were then isolated from the **B1**−**B5** fractions by an affinity method using anti-IAF mAb affinity resin[7] (steps e, f, Figure 1) and examined by LC/MS (step g, Figure 1). Using this process, the IAF probe **3** was identified with an exact mass of *m/z* 1024.3012 in the nuclear (**C1**), *m/z* 1024.3005 in the cytosolic (**C3**), and *m/z* 1024.3021 in the mitochondrial-perioxome-lysosomal (**C5**) fractions. The distribution of probe **3** in three of the five fractions indicated that its isolation was guided by affinity to the protein content of the resins and not by unspecific interactions with the resin. Probe **3**[11] remained active and delivered a mitotic block ∼1000-fold greater than the parent crude extracts when reassayed in cell culture (HeLa, IC_{50} value of 1.6 ± 0.2 nM; HCT116, IC_{50} value of 3.2 ± 0.3 nM cells; Neuro-2a, IC_{50} value of 1.2 ± 0.2 nM).

Next, we developed a preparative method to isolate the natural product precursor to probe **3** by analyzing the active fractions through IAF-labeling and LC/MS analysis (steps h−m, Figure 1).[12] Consequently, a total of 21.2 mg of (±)-laetirobin (**1**) was isolated from the *Laetiporus* specimens XRI2009 and XRI2132. In order to eliminate the possibility that (±)-laetirobin (**1**) arose from the method of extraction, we collected 8.6 mL of sap by milking a specimen of *L. sulphureus* (specimen XRI3129) growing on *R. pseudoacacia*. The sap was collected over a 2 h period and immediately frozen in liquid nitrogen, freeze-dried, and directly purified (steps h−m, Figure 1) to provide 1.2 mg of (±)-laetirobin (**1**). This observation indicated that **1** was indeed present in the parent organism and did not occur during the extraction process. Pure (±)-laetirobin (**1**) displayed potent cytostatic activity (HeLa, IC_{50} value of 0.12 ± 0.05 nM; HCT116, IC_{50} value of 0.54 ± 0.09 nM; Neuro-2a, IC_{50} value of 0.092 ± 0.031 nM) that led to cell

* To whom correspondence should be addressed. Tel: +001-858-401-3083. E-mail: i@xenobe.org. Tel: +65-6516-3998. E-mail: chmlmj@nus.edu.sg.
† National University of Singapore.
‡ University of California, San Diego.
§ Salk Institute for Biological Studies.
∞ Xenobe Research Institute.

10.1021/np9002838 CCC: $40.75

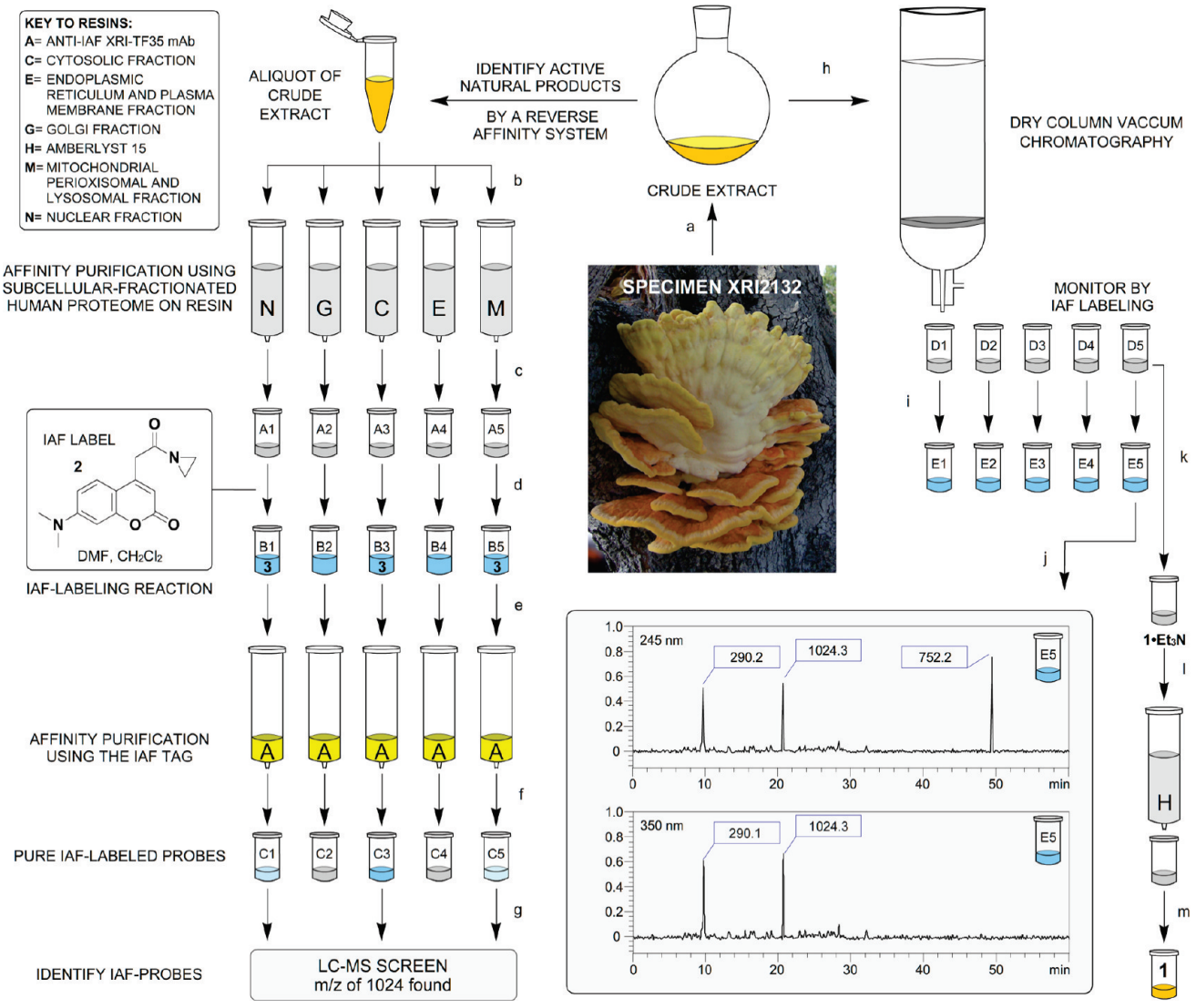

Figure 1. Affinity-guided identification and isolation of (±)-laetirobin (**1**). Steps: (a) Crude extracts from *L. sulphureus* specimens were prepared, dried, and dissolved in 100 mL of PBS pH 7.2 containing 0.5% DMSO. (b) Each extract solution was circulated through a series of five subcellular-fractionated proteomic resin columns N, G, C, E, and M for 12 h at 4 °C, then purged with PBS pH 7.2 and H_2O. (c) Each column was removed from the system, and the bound materials were eluted with warm 95% EtOH. (d) The resulting dried fractions **A1**−**A5** were treated with IAF label **2**[8] to afford fractions **B1**−**B5**. (e) Fractions **B1**−**B5** in 25 mL of RIPA buffer containing 0.8% DMSO were passed through resin A containing 5.0 ± 0.1 mg/mL of XRI-TF35 mAb,[7] a mouse immunoglobulin G (IgG) against the IAF-label. (f) Resin A was washed with PBS pH 7.2 and water, and the bound materials were eluted with warm 95% EtOH. (g) The resulting fractions **C1**−**C5** were screened for absorption of the IAF label at 350 nm by LC/MS; fractions **C1**, **C3**, and **C5** from XRI2009 or XRI2132 gave IAF probe **3** (*m*/*z* 1024.3012). (h) Extracts from the remaining XRI2009 (1.8 g) and XRI2132 (2.1 g) specimens were purified by dry-vacuum column chromatography to afford fractions **D1** (2:1 hexanes/EtOAc), **D2** (1:1 hexanes/EtOAc), **D3** (EtOAc), **D4**, (1:10 MeOH/EtOAc), and **D5** (1:2:0.2 MeOH/EtOAc/Et_3N). (i) Aliquots of **D1**−**D5** were dried and conjugated with IAF label **2** to afford **E1**−**E5**. (j) Probe **3** (*m*/*z* 1024) was found in **E5** by LC/MS analysis, implying that the natural precursor **1** was in fraction **D5**. (k) Crystallization of fraction **D5** afforded **1**·Et_3N. (l) Passage of **1**·Et_3N through Amberlyst-15 resin and (m) crystallization from 1:1 $CHCl_3$/MeOH afforded 12.8 mg of **1** (from XRI2009) and 8.4 mg of **1** (from XRI2132). While the HPLC traces indicate a high purity of **1** in fraction **D5/E5** at 245 and 350 nm absorbences, subsequent ion exchange and recrystallization were required to obtain **1** in pure form, as both metal ion (predominantly sodium) and triethylammonium salts were obtained after DCVC purification.

death, and **1** displayed comparable cellular phenotypes to probe **3** and the parent crude extracts of XRI2009 and XRI2132.

High-resolution EIMS provided an exact mass of *m*/*z* of 752.1882 and 752.1874 from the respective samples for XRI2009 and XRI2132. We searched for ions with *m*/*z* 752.1882 and 752.1874 with Xcalibur (ThermoScientific) and obtained 57 matching elemental formulas within a delta of 25 amu.[13] Each of the masses identified in this search contained an H/C ratio of 0.78 or less (0.54 on average). While each of the formulas contained over 40 carbon and 25 hydrogen atoms, the ^{1}H NMR spectrum of **1** was remarkably simple (Figure 2a), suggesting that elucidation of the structure of **1** by NMR methods may be ambiguous.

Examination of the ^{1}H NMR spectrum indicated that two singlets corresponding to phenolic hydroxyl groups were apparent at δ 12.40−12.60 (Figure 2b) and exchanged upon addition of methanol-d_4. A total of 10 singlets were observed between δ 6.10 and 8.10 (Figure 2c), and three additional singlets appeared at δ 2.20−3.00 (Figure 2d). Only two spin systems existed, with a triplet at δ 4.47 and a complex multiplet spanning δ 2.30−2.80 (Figure 2d). The appearance of these two spin systems was further confirmed by gCOSY (Figure 2i) and TOCSY (Figure 2j) spectra. The ^{13}C NMR resonances were observed clustered in repeating peaks (Figure 2e−h), suggesting that the structure of **1** was composed of three to four monomeric units. This was further confirmed by repeating sets

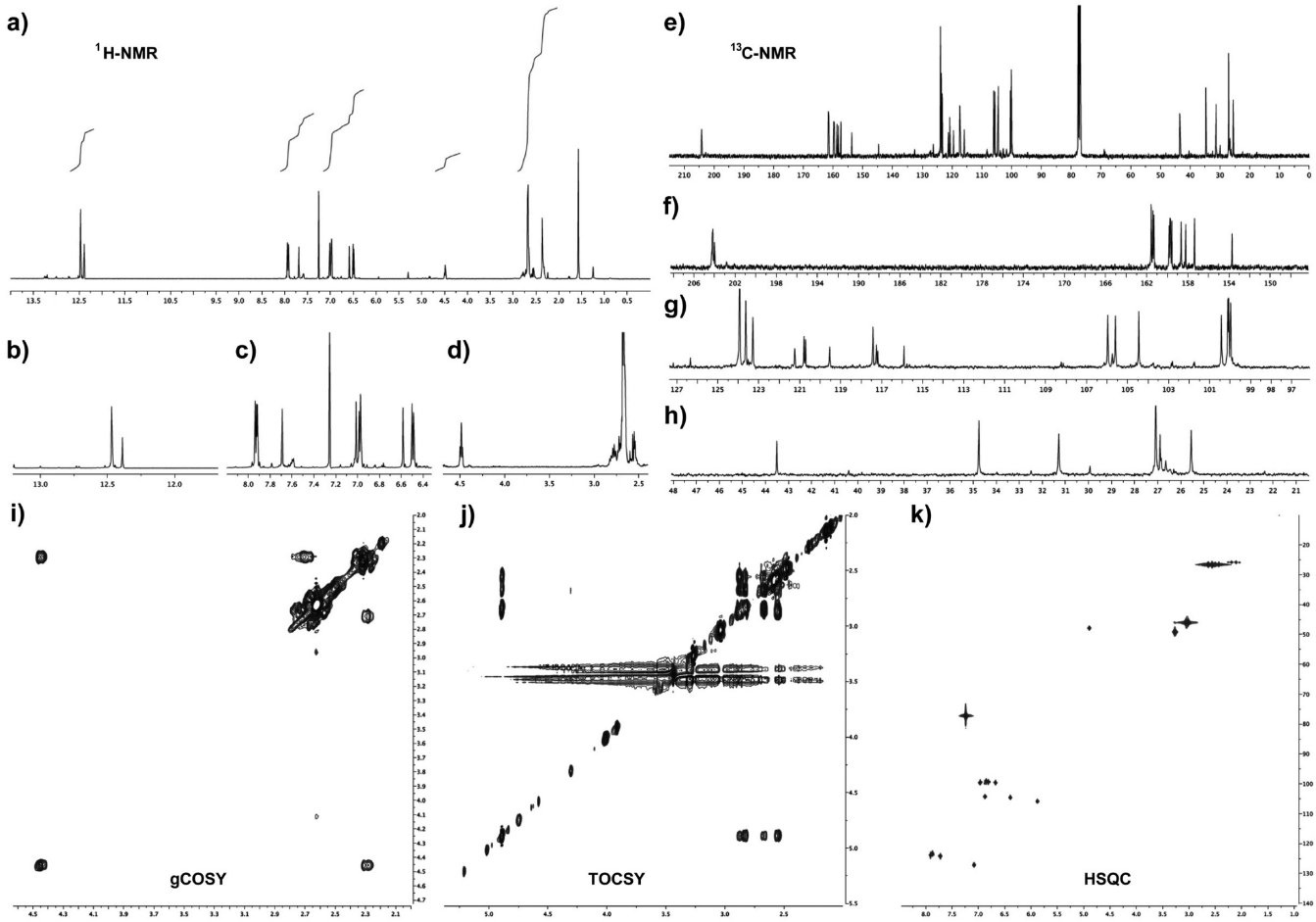

Figure 2. Selected NMR data from (±)-laetirobin (**1**). (a−k) NMR studies on (±)-laetirobin (**1**) confirmed a repeating benzofuran motif. (a−d) 500 MHz ^{1}H NMR spectrum of **1**. (e−h) 125 MHz ^{13}C NMR spectrum of **1**. (i) 500 MHz gCOSY spectrum of **1**. (j) 800 MHz TOCSY spectrum of **1**. (k) 800 MHz HSQC spectrum of **1**.

Table 1. NMR Spectroscopic Data (500 MHz, $CDCl_3$) for 1-(6-Hydroxybenzofuran-5-yl)ethanone (**4**)[a]

position	δ_C, mult.	δ_H (J in Hz)	gCOSY	TOCSY	ROESY	HMBC[b]
1	204.29, qC					
2	27.07, CH_3	2.67 s				1,4′,5′
2′	145.79, CH	7.53 d (2.0)	3′	3′		3′,3a′,7′,7a′
3′	106.82, CH	6.70 d (2.0)	2′	2′,7′		2′,3a′,4′,7a′
3a	120.42, qC					
4′	124.02, CH	7.97 s				1,2′,3′,5′,6′,7′,7a′
5′	117.23, qC					
6′-OH		12.39 s				1,5′,6′,7′,7a′
6′	161.10, qC					
7′	100.04, CH	7.00 s		3′		1,3a′,4′,5′,6′,7a′
7a′	159.77, qC					

[a] The assignments of H and C residues were made by a combination of gCOSY, TOCSY, NOESY, HSQC, and HMBC analyses. [b] HMBC correlations, optimized for 8 Hz, are from δ_H to δ_C.

of peaks within the HSQC spectrum (Figure 2k). These data and subsequent HMBC spectra (Table 2) suggested that the unit was 1-(6-hydroxybenzofuran-5-yl)ethanone (**4**), as depicted in Figure 3a.

To confirm these NMR assignments, we synthesized benzofuran **4** from 2,4-dihydroxyacetophenone using the approach of Goel.[14] NMR studies indicated a comparable position of the ^{1}H and ^{13}C NMR residues in **4** (Table 1) in relation to **1** (Table 2). We were now able to assign regions of the aromatic residues by direct comparison of **4** to **1**. There was also a direct correlation in the position of ^{13}C NMR peaks in the aromatic region of **1** with those in **4**, thereby providing further support for the assignment. In addition, the benzophenone units in compound **1** lacked the C-2 and C-3 coupling apparent in **4** (cf. Tables 1 and 2). This, along with the comparative positions of the ^{1}H and ^{13}C NMR residues, suggested that three benzofuran moieties were attached via the C-2 carbon in **4**. Extension of this evaluation indicated that a fourth benzofuran unit was contained in bonds at both C-2 and C-3 carbons of **4**. With this evidence, we were confident that the structure of **1** was comprised of four molecules of **4**, three linked through C-2 and one via C-2 and C-3.

In the process of gaining further long-range interactions by collecting a *J*-resolved HMBC spectrum over 48 h, compound **1** crystallized from a 1:10 methanol-d_4/$CDCl_3$ mixture. Although this prevented NMR data acquisition, X-ray crystallographic measurements on the resultant small yellow triclinic crystals revealed a unique framework, comprising four units of benzofuran **4** contributing to a six-membered ring (Figure 3b). Using this X-ray structure,

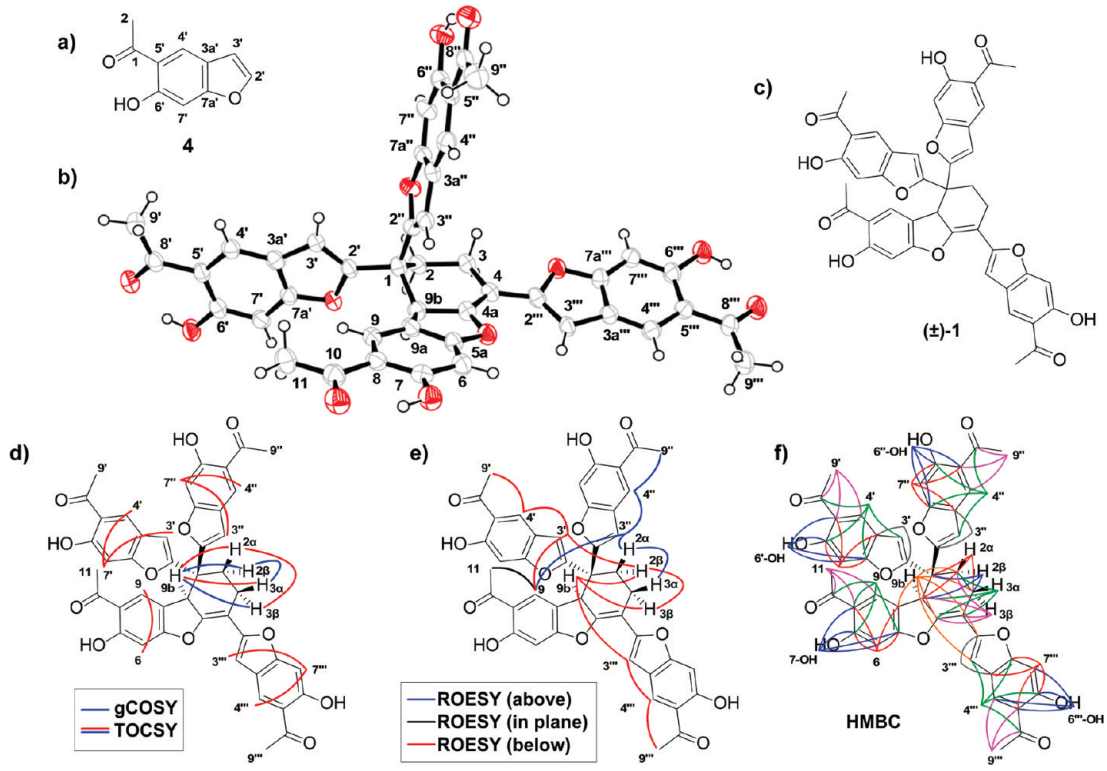

Figure 3. Selected structural information. (a) Structure of 1-(6-hydroxybenzofuran-5-yl)ethanone (**4**). (b) X-ray crystal structure of (±)-laetirobin (**1**). (c) Structure of (±)-laetirobin (**1**). NMR interactions of **1** by (d) gCOSY (blue) and TOCSY (red and blue), (e) ROESY (colored according to position on, above, or below the XY plane of **1**), and (f) HMBC (interactions colored for clarity) analyses.

we completed the assignments of each hydrogen and carbon residue (Table 2). These data were then checked for validity by examining 2D interactions in the gCOSY (Figure 3d), TOCSY (Figure 3d), ROESY (Figure 3e), and HMBC (Figure 3f) data. Several salient features in this data set were in direct agreement with the crystal structure. First, the five aliphatic hydrogens at C-2, C-3, and C-9b displayed the expected vicinal and long-range couplings in the gCOSY and TOCSY spectra. The key hydrogen at C-9b was observed as a triplet at δ 4.47 with two homoallylic 5.5 Hz couplings to the two protons at C-3 in the gCOSY spectrum (Table 2) and correlations to the four hydrogens at C-2 and C-3 in the TOCSY spectrum (Figure 3d). The hydrogens at C-2 and C-3 also displayed the expected vicinal couplings (Table 2), which were further supported by strong NOEs between the noncoupling adjacent hydrogens in the ROESY spectrum (Figure 3e). Further long-range NOEs were also in accordance with this structure including (i) a direct correlation between the α- and β-hydrogens at C-2 with the corresponding hydrogen at C-3′ or C-3″ as well as a correlation between the hydrogen at C-9 and (ii) the hydrogens at C-3′ or C-3″ (see further Figure 3d and Table 2). These correlations allowed the assignment of the proton and carbon resonances on the two faces of the molecule, given the interactions of the α-protons at C-2 and C-3 with one of the aryl-containing C-3′ and β-protons at C-2 and C-3 with C-3″. The correlation between C-9b and the α-proton at C-2 confirmed these assignments.

Finally, the HMBC data provided strong support for each of the fragments, with each proton showing multiple interactions with neighboring carbon atoms (Figure 3f). The observed high-resolution masses of *m*/*z* of 752.1882 and 752.1874 matched that of (±)-laetirobin (**1**), with a chemical formula of $C_{44}H_{32}O_{12}$ and expected mass *m*/*z* of 752.1894.

It should be noted that all samples of (±)-laetirobin (**1**) were optically inactive, $[\alpha]_D^{20} = 0.04 \pm 0.01$. This observation indicated that either the biosynthesis of **1** afforded both enantiomers (Scheme 1), thereby suggesting that **1** did not form in an enzyme pocket, or single enantiomers of **1** were produced through an enzymatic Diels−Alder reaction that racemized during isolation. Treatment of compound **1** in methanol-d_4 with NaOD or Et_3N (used during purification) led to the exchange of not only the phenolic hydrogens but also the hydrogen at C-9b (as evidenced by loss of the assigned signal at δ 4.47). These observations support equilibration of the C-9b hydrogen, and thus racemization could have occurred during isolation, but do not necessarily support an enzymatically controlled synthesis of laetirobin, as depicted in Scheme 1.

We then turned to imaging studies in order to characterize the cellular activity of **1**. Our initial plan was to prepare IAF probes of the natural product for cellular and molecular target studies.[7b] Interestingly, during our earlier screening studies (Figure 1), the blue-fluorescent probe **3** also displayed fluorescence in the red and green channels. Independent studies confirmed this fluorescence to arise from the natural product, thereby allowing live cell imaging to be performed with unlabeled **1**. We therefore postponed studies with probe **3**[11] and focused our attention on examining the uptake and localization of **1**.

Using fluorescence densitometry to quantify the cell uptake,[15] we determined that **1** reached an intracellular saturation of ~10 μM within 15 min upon the addition of 500 μL of 1 nM **1** to a 35 mm diameter dish containing 10^6 cells/cm^2. Repeated washes with media followed by live cell imaging, or by formalin fixation, returned intracellular concentrations of 0.5−5 μM **1** within the HeLa, HCT116, and Neuro-2a cell lines studied. While concentration variances were due to the cell line used, media, and length of incubation, this result indicated that (±)-laetirobin (**1**) concentrated up to 5000-fold in tumor cells from the extracellular media. During this process, the subcellular localization of **1** remained constant. The native fluorescence from **1** was multicolored with blue or red fluorescence predominating in the nuclear envelope (ne, Figure 4a and e) and large vesicles (ve, Figure 4a; costaining with LysoTracker Red DND-99[16] confirmed these to be lysosomes). Through spectrophotometric measurements, the green fluorescence from **1** at 530 nM was shown to increase with acidity in the lysosomes (Figure 4f).

Table 2. NMR Spectroscopic Data (500 MHz, $CDCl_3$) for (±)-Laetirobin (**1**)[a]

position	δ_C, mult.	δ_H (*J* in Hz)	gCOSY	TOCSY	ROESY	HMBC[d]
1	43.5, qC					
2[b]	31.3, CH_2	2.71 m	3	3,9b	3α,3″	1,3,9b[c]
2[b]		2.76 m	3	3,9b	3*β*,3′,9b[c]	1,3,9b[c]
3[b]	25.5, CH_2	2.36 m	2,9b	2,9b	2α	2[c],4[c],4a[c],9b[c]
3[b]		2.32 m	2,9b	2,9b	2,9b	2[c],4[c],4a[c],9b[c]
4	144.7, qC					
4a	153.7, qC					
5a	159.6, qC					
6	100.4, CH	7.00 s		9		5a,7,8,9a
7	161.3, qC					
7-OH		12.37 s				5a,6,7,8
8	115.9, qC					
9	123.3, CH	7.68 s		6	11,3′,3″	5a,7,8,10
9a	119.5, qC					
9b	34.7, CH	4.47 t (5.5)	3,3	2,2,3,3	2*β*[c],3*β*,3‴	2,3,4a,9a,2‴,3‴
10	204.0, qC					
11	26.9, CH_3	2.35 s			9	8,9,10
2′	158.7, qC					
3′	106.0, CH	6.48 s		7′	2,9,4′	2′,3a′
3a′	120.7, qC					
4′	123.9, CH	7.91 s		7′	3′,9′	3′,6′,7a’,8′
5′	117.2, qC					
6′	161.5, qC					
6′-OH		12.45 s				5′,6′,7′,7a′
7′	100.1, CH	6.96 s		3′,4′		3a′,5′,6′,7a′
7a′	159.7, qC					
8′	204.2, qC					
9′	27.1, CH_3	2.65 s			4′	4′,5′,8′
2″	158.2, qC					
3″	105.7, CH	6.57 s		7″	2,9,4″	2″,3a″
3a″	120.8, qC					
4″	123.9, CH	7.92 s		7″	3″,9″	3″,6″,7a″,8″
5″	117.2, qC					
6″	161.5, qC					
6″-OH		12.45 s				5″,6″,7″,7a″
7″	100.1, CH	6.96 s		3″,4″		3a″,5″,6″,7a″
7a″	159.7, qC					
8″	204.2, qC					
9″	27.1, CH_3	2.65 s			4″	4″,5″,8″
2‴	157.3, qC					
3‴	104.4, CH	6.47 s		7‴	9b,4‴	2‴,3a‴
3a‴	121.2, qC					
4‴	123.6, CH	7.90 s		7‴	3‴,9‴	3‴,6‴,7a‴,8‴
5‴	117.4, qC					
6‴	161.4, qC					
6‴-OH		12.44 s				5‴,6‴,7‴,7a‴
7‴	100.0, CH	6.97 s		3‴,4‴		3a‴,5‴,6‴,7a‴
7a‴	159.8, qC					
8‴	204.1, qC					
9‴	27.1, CH_3	2.66 s			4‴	4‴,5‴,8‴

[a] The assignments of C′, C″, and C‴ as well as H′, H′, and H‴ are based on a combination of gCOSY, TOCSY, NOESY, HSQC, and HMBC analyses. [b] The assignments of α and *β* protons have not been confirmed. [c] Weak correlations. [d] HMBC correlations, optimized for 8 Hz, are from δ_C.

Time-lapse microscopy indicated that the cells, which were blocked during mitosis, transitioned into an apoptotic state. These cellular transformations were characterized by membrane scarring (chromatin agglomeration) between two daughter cells (dc, Figure 4d) and bleb formation (bl, Figure 4c). This response was also observed in HeLa and HCT116 cells. Subcellular components of the cells locked by (±)-laetirobin (**1**) were further examined by fixing with formalin, after which the microtubules and actin were counterstained with BODIPY-FL paclitaxel[17] and FITC-phalloidin,[18] respectively. Analyses by confocal microscopy consistently revealed severe hyperfilamentation of actin (green, Figure 4d) and disassociation of microtubule structures (red, Figure 4d) in each cell line. Using a motionless bench, these effects were shown to occur directly upon blockage during mitosis and were not an artifact of mechanical disruption.

The uptake and subcellular localization of **1**, late-stage mitotic block, and evidence of entry into apoptosis suggests that (±)-laetirobin (**1**) targets growth-related processes that collectively differ from known antimitotic agents.[19] Its structure is a novel fusion of four benzofuran moieties that is distinct from related benzofuran-containing natural products isolated from *L. sulphureus*,[5c] other fungi, or plants.[20] Important to the discovery of this cytostatic lead was the application of our IAF labeling system,[8] purpose-built to identify natural products with an innate ability to associate with proteins actively expressed in human cancer cells (i.e., HeLa). Our proteome-guided, reverse-affinity platform not only expedited the identification of a compound with relevant biological activity but also furnished a molecular probe (i.e., probe **3**) in harmony with isolation work. Studies are underway to apply these materials, as well as materials from a biomimetic total synthesis,[21] to identify the molecular targets of (±)-laetirobin (**1**) and to elucidate their role within the observed transitions during cell division and programmed cell death.

Experimental Section

General Experimental Procedures. Optical rotations were determined on a Perkin-Elmer-241 MC polarimeter. UV−vis spectra were collected on a PTI QuantaMaster UV−vis Steady State spectrofluo-

Scheme 1. Proposed Biosynthetic Origin of (±)-Laetirobin (**1**)[a]

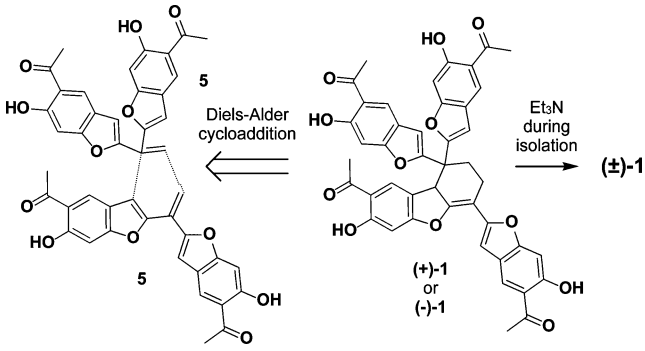

[a] The biosynthesis of **1** may arise through a homodimeric Diels−Alder dimerization of an alkene precursor **5**. This process could either occur without enzymatic acceleration to afford (±)-**1** or arise through enzymatic action to give a single enantiomer of **1**, which is subsequently isomerized to (±)-**1** during the isolation process due to the use of Et_3N.

rometer with a 0.1 cm quartz cell at 23 °C. FT-IR spectra were collected using a thin film on a Perkin-Elmer Spectrum One FTIR spectrometer. Mass spectra were obtained by Dr. Yongxuan Su at the UCSD Department of Chemistry and Biochemistry Mass Spectrometry Facility, with HRMS spectra collected on a ThermoFinnigan MAT900XL-MS. NMR spectra were recorded on a Varian Mercury 400, Bruker DMX500, Varian 500, or Bruker Avance 800 spectrometer, as noted herein. Samples were dissolved in $CDCl_3$, and chemical shifts were calculated relative to the $CDCl_3$ solvent peak (δ_H at 7.24 and δ_C at 77.23). HMBC spectra were collected at $J_{1,3} = 3$, 8, 10, and 12 Hz, with HMBC spectra from measurements at $J = 8$ Hz displayed throughout. NMR spectra were processed with MestreNova (*MestreNova*, Version 5.2.5-4119, Mestrelab Research S. L., Santiago de Compostela, Spain). Solvents were purchased from VWR Scientific or Fisher Scientific and used as is. Unless otherwise noted, solvent ratios are noted in v/v. LC/MS analyses were conducted from multiple instruments, columns, and solvent mixtures. A typical procedure is described using an Agilent 1100 LC with an Xterra reversed-phase column (50 × 4.6 mm, 1 × d) with matching guard cartridge (Waters). Typical LC assay conditions: mobile phase A: 0.1% HCO_2H in H_2O, B: 0.1% HCO_2H in CH_3CN, gradient = 5−95% B in 12.5 min; 1.5 mL/min A/B with post-column injection of C: 20 mM NH_4OAc in CH_3CN/H_2O (3:1), 0.2 mL/min; 2.5 μL injection volume (1.0−5.0 μM sample); DAD detection monitored at 254 nm plus up to two additional wavelengths, including IAF-tag-specific absorption at 350−365 nm. The masses of the identified peaks were determined by collection of the eluant followed by MS analysis or by direct LC/MS analysis.

Subcellular Fractionation. Two methods were used to prepare the subcellularly fractionated protein lysates. Ultracentrifugation was used to prepare HeLa cell fractions containing the nuclei for resin N (step b, Figure 1); the cytosol for resin C (step b, Figure 1); the endoplasmic reticulum and plasma membranes for resin E (step b, Figure 1); and the mitochondria, lysosomes, and peroxisomes for resin M (step b, Figure 1). The Golgi fraction for resin G (step b, Figure 1) was prepared separately. General procedure: A frozen and thawed pellet of HeLa cells was suspended at 50 mL/g of cells in lysis buffer containing phosphate-buffered saline (PBS) pH 7.2, 1% Triton X100, and 0.1% SDS. The cells were ruptured by repeated passage through a 28-gauge needle. A nuclei pellet was collected after centrifugation at 800*g* for 10 min. A pellet containing mitochondria, lysosomes, and peroxisomes was collected after centrifugation of the remaining supernate at 15000*g* for 10 min. The endoplasmic reticulum and plasma membrane were pelleted after centrifugation of the remaining supernate at 100000*g* for 60 min. Each pellet was diluted with lysis buffer containing PBS pH 7.2, 1% Triton X100, 0.1% SDS, and a protease inhibitor cocktail (Sigma-Aldrich), ruptured by ultrasonification, and concentrated to 5 mg/mL in net protein by spin dialysis on a 9 kDa MWCO iCON spin concentrator (Pierce). The cytosol fraction was obtained after collecting the supernate after 200000*g* for 3 h followed by concentration to 5 ± 0.2 mg/mL in net protein spin dialysis on a 9 kDa MWCO iCON spin concentrator. The Golgi fraction (for resin G, Figure 1) was collected from HeLa cells by use of a Golgi isolation kit (Sigma-Aldrich). A lysate was prepared from the Golgi fraction via homogenolysis by ultrasonification followed by concentration to 5 mg/mL in net protein spin dialysis on a 9 kDa MWCO iCON spin concentrator. Each fraction was either dialyzed or spin dialyzed into 50 mM MOPS, 150 mM NaCl, and 10 mM $MgCl_2$ buffer for resin coupling.

Affinity Resin Preparation. Preparation of subcellularly fractionated reverse-affinity resins: Reverse affinity resins N, G, C, E, and M (Figure 1) were prepared by washing Affi-Gel 10 resin with an equal volume of EtOH (2×), 50% EtOH (2×), and PBS pH 7.2 at 4 °C. Immediately after washing, the subcellularly fractionated lysate containing 5 mg/mL in net protein was added, and the resin was shaken for 6 h at 4 °C. One resin was prepared for each of the five subcellular fractions (N, G, C, E, and M, Figure 1). After loading of the lysate protein, each resin was filtered and capped by treatment with an equal volume of 100 mM glycine ethyl ester in PBS at pH 7.2 containing 10 mM $MgCl_2$ for 3 h at 4 °C. The resin was harvested and washed three times with 1 mL of PBS at pH 7.2 containing 10 mM $MgCl_2$. The protein concentration on each resin was determined either by A_{280} measurement or commercial protein quantification kits (Bio-Rad). Each resin was stored at 4 °C in PBS at pH 7.2 containing 10 mM $MgCl_2$ up to 24 h prior to use.

Preparation of Anti-IAF Affinity Resin. The anti-IAF Affi-Gel Hz resin A (Figure 1) was prepared with modest modification of the Affi-Gel Hz resin kit (Bio-Rad). The procedure started by oxidation of the XRI-TF35 mAb, an antibody elicited with affinity to the 7-dimethyaminocoumarin-4-acetamide (IAF) label.[7] The XRI-TF35 mAb was transferred to coupling buffer pH 5.5 (Bio-Rad) by repetitive dilutions on 9 kDa iCON spin filters to deliver a final concentration of 4.9−5.1 mg/mL mAb, as determined by Bradford analysis.[22] A 1 mL aliquot of solution was diluted in 5 mL of coupling buffer pH 5.5 (Bio-Rad) and oxidized by addition of 500 μL of freshly prepared solution of 30 mg/mL $NaIO_4$ (Sigma-Aldrich) in water. This solution was rotated with inversion for 1 h, at which point the salts were removed by spin concentration at 4 °C with six successive equivalents of coupling buffer on a 9 kDa iCON spin filter to deliver a final concentration of 4.9−5.1 mg/mL mAb, as determined by Bradford analysis.[22] The oxidized mAb was coupled to washed Affi-Gel Hz resin by shaking the slurry for 12 h at 23 °C followed by equilibrating by washing three times with two volumes of PBS. The loading of protein on the resin was determined by A_{280} measurements or commercial protein quantification kits (Bio-Rad).

Extract Preparation. Fruiting bodies were collected from *L. sulphureus* in parasitic growth on *E. cladocalyx* (specimen XRI2018, 1.21 kg; specimen XRI2022, 0.92 kg), saprobic growth on *E. cladocalyx* (specimen XRI2102, 0.85 kg), saprobic growth on *Q. dumosa* (specimen XRI2011, 0.34 kg), parasitic growth on *Q. dumosa* (specimen XRI2032, 0.92 kg), and parasitic growth on *R. pseudoacacia* (specimen XRI2009, 1.95 kg; specimen XRI2132, 0.42 kg). The identification was conducted by one of the authors (J.J.C.) using both spore and structural analyses. Voucher samples of *L. sulphureus* are deposited at the Xenobe Research Institute in San Diego, CA, and can be provided upon request. The mushrooms were frozen at −78 °C and stored at −20 °C after collecting. A total of seven extracts were prepared using an identical procedure to process each specimen. Fungal fruit bodies were broken into 100−300 cm^2 squares and soaked in absolute EtOH (1 L per kg of wet mass) for 24 h at 4 °C. The EtOH was filtered through a coarse sintered glass funnel and concentrated by rotary evaporation. The crude extract was partitioned between a 1:2 (v/v) mixture of CH_3CN/hexanes. The CH_3CN layer was collected and dried via rotary evaporation to deliver a crude extract.

Identification of (±)-Laetirobin (1). A seven-step procedure (steps a−g) was used to identify the natural product as depicted in Figure 1. A 300 mg sample of a crude extract was dissolved in 500 μL of DMSO, diluted to 100 mL in PBS (pH 7.2), and filtered through a 0.2 μm syringe filter (Whatman). A polycarbonate-fritted column (Ridout Plastics) was charged with 15 mL of the subcellular fractionated reverse-affinity resins. Five of these columns, one for each resin, were attached in series using Tygon tubing (Figure 1). The system was then charged with the extract solution (300 mg of crude extract in 100 mL of PBS pH 7.2). This solution was then pumped through each resin cartridge with a low-pressure liquid diaphragm pump (KNF-Neuberger) at a flow rate of ∼0.5 mL/min for 12 h at 4 °C (step b, Figure 1).

After this period of binding, the extract solution was removed from the system. The resins were washed by pumping the system twice with PBS pH 7.2 and twice with H_2O. The columns were then removed

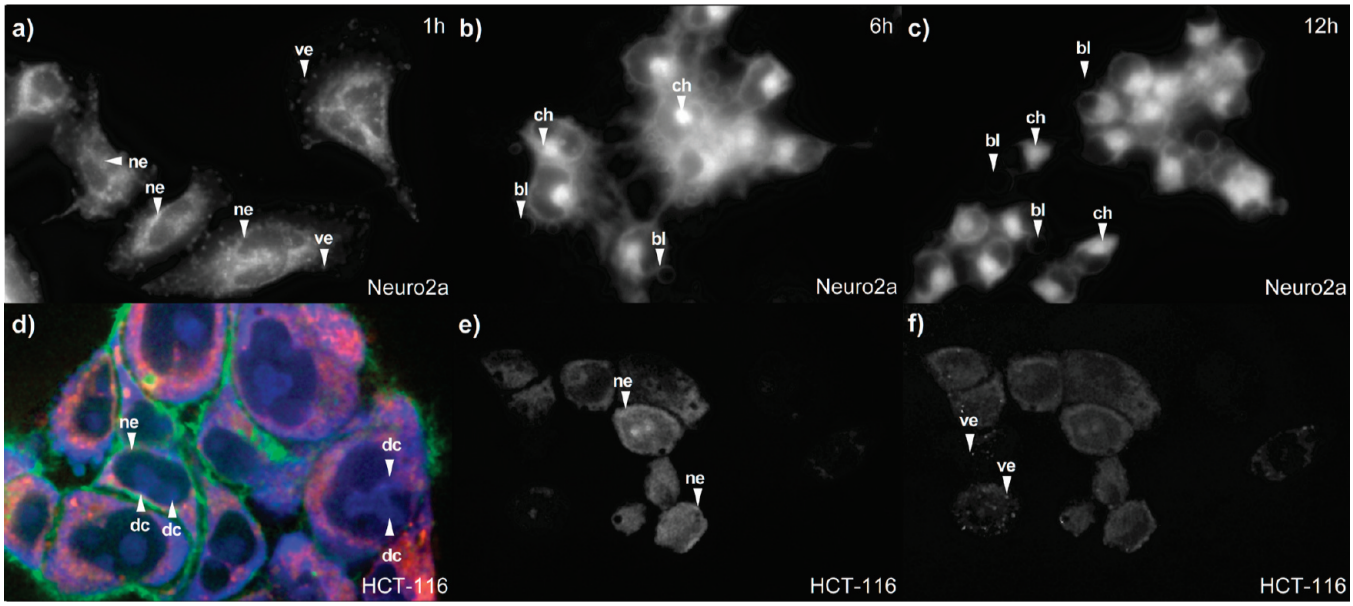

Figure 4. Effects of (±)-laetirobin (**1**) on tumor cell growth and proliferation. (±)-Laetirobin (**1**) localizes in Neuro-2a cells, blocks cell division, and induces apoptosis. (a) Neuro-2a cells 1 h after the treatment with 1 nM **1** display native fluorescence from **1** in nuclear envelope (ne) and vesicles (ve). Cells cultured in the absence of **1** were not fluorescent and underwent normal cell growth and division (not shown). Neuro-2a cells form blebs (bl) and compact their chromatin (ch) after (b) 6 h and (c) 12 h after treatment with 1 nM **1**. Images depict the native fluorescence from **1**. (d) Confocal microscopy image of HCT116 cells treated with 1 nM **1** prior to entrance into mitosis followed by staining of their microtubules (red), actin (green), and DNA (blue). Cells treated with 1 nM **1** failed to complete mitosis, as characterized by incomplete separation of daughter cells (dc). (e, f) Confocal microscopic analysis of HCT116 cells reveals the multicolor fluorescence from **1**. (e) Red fluorescence appears in the nuclear envelope (ne), while (f) green fluorescence appears within vesicles (ve).

from the system. The bound materials were eluted from each column using 95% EtOH warmed to 50 °C and dried under vacuum to afford fractions A1−A5 (step c, Figure 1). One fraction was obtained from each column. Fractions A1−A5 were then labeled with an IAF tag (step d, Figure 1). This was accomplished by dissolving fractions A1−A5 at 1 mg/mL in an anhydrous mixture of 1:1 CH_2Cl_2/DMF and treating these solutions with an equivalent volume of 5 mg/mL solution of tag **2**[8] in anhydrous DMF. After 12 h at 4 °C, the reaction was terminated by the addition of 100 μM Me_2NH. The resulting solutions were then dried under vacuum to afford fractions B1−B5 (step d, Figure 1). Fractions B1−B5 were then dissolved in 200 μL of DMSO and diluted in 25 mL of RIPA buffer (25 mM Tris pH 7.6, 150 mM NaCl, 1% NP-40, 1% sodium deoxycholate, and 0.1% sodium dodecyl sulfate, SDS). The five IAF-labeled materials were purified from this mixture using an immunoaffinity method (step e, Figure 1). The five crude IAF-labeled fractions were passed individually through affinity columns containing 0.5 mL of anti-IAF affinity resin A.

After incubation for 12 h at 4 °C, the samples of resin A were washed three times with 50 mL of RIPA buffer and twice with 50 mL of H_2O. The bound materials were eluted by washing each column with 95% EtOH at 50 °C and drying the eluted fractions under vacuum to afford fractions C1−C5 (step f, Figure 1). Fractions C1−C5 were dissolved at 10 mg/mL in DMSO then evaluated by LC/MS analysis. Fractions containing IAF-labeled probe **3** with *m*/*z* 1024 were collected (step g, Figure 1).

X-ray Crystallography. A crystal structure was collected on a crystal of **1**. A copy of the coordinates for this structure has been uploaded to the Cambridge Crystallographic Data Centre (http://www.ccdc.cam.ac.uk/). Crystals were mounted on glass fibers. X-ray data were collected with a Bruker AXS SMART APEX diffractometer, using Cu Kα radiation at 100 K with the SMART suite of programs (*SMART*, version 5.628, Bruker AXS, 2001). Data were processed and corrected for Lorentz and polarization effects with SAINT (*SAINT+*, version 6.22a, Bruker AXS Inc., Madison, WI, 2001) and for absorption effect with SADABS (Sheldrick, G. W. *SADABS*, version 2.10, University of Goettingen, Germany, 2001). Structural solution and refinement were carried out with the SHELXTL suite of programs (*SHELXTL*, version 6.14, Bruker AXS, 2000). The structure was solved by direct methods to locate the heavy atoms, followed by difference maps for the light, non-hydrogen atoms. All non-hydrogen atoms were generally given anisotropic displacement parameters in the final mode. All H atoms were placed at calculated positions. A very small yellow block of compound **1**, 0.08 × 0.04 × 0.04 mm, was used for data collection at 100(2) K using Cu Kα radiation, and 12 232 reflections were collected, 5953 of which were unique (R_{int} = 0.069). No symmetry higher than triclinic was observed, and the centrosymmetric alternative, $P\bar{1}$, was chosen on the basis of the results of refinement. Direct methods were used to solve the structure, and all non-hydrogen atoms were refined anisotropically. All H atoms were placed in idealized locations. The asymmetric unit contains a molecule of $CHCl_3$. For $C_{45}H_{33}Cl_3O_{12}$, triclinic, $P\bar{1}$, a = 10.8711(10) Å, b = 13.8138(12) Å, c = 14.0844(13) Å, α = 112.142(6)°, β = 90.894(6)°, γ = 94.006(6)°, V = 1952.3(3) Å^3, Z = 2, D_x = 1.483 Mg/m^3, R1 = 0.0694, wR2 = 0.1746 based on 2σ(I) data.

Preparative Isolation of (±)-Laetirobin (1). The 1024 *m*/*z* peak identified as probe **3** during reverse-affinity purification was used to guide preparative isolation of the active natural product (steps h−m, Figure 1). The XRI2009 or XRI2132 in CH_2Cl_2 were fractionated by dry vacuum chromatography on a 20 cm high by 20 cm i.d. column loaded with silica gel 60 (0.015−0.04 mm) by the successive passing of 600 mL aliquots of 2:1 hexanes/EtOAc, 1:1 hexanes/EtOAc, EtOAc, 1:10 MeOH/EtOAc, and 1:2:0.2 MeOH/EtOAc/Et_3N. An aliquot of each of the resulting fractions was fluorescently labeled (Figure 1i) and subjected to LC/MS analysis. This was accomplished by dissolving each material at 1 mg/mL in an anhydrous mixture of 1:1 CH_2Cl_2/DMF and treating these solutions with an equivalent volume of 5 mg/mL of tag **2** in anhydrous DMF. The 1024 *m*/*z* peak appeared in the 1:2:0.2 MeOH/EtOAc/Et_3N fraction (Figure 1j). This fraction contained an ∼80% pure sample of the triethylammonium salt of laetirobin (**1**·Et_3N) as judged by NMR and was crystallized by slow evaporation of 10:1:0.1 CH_2Cl_2/MeOH/Et_3N (step k, Figure 1). This material was readily converted to **1** by passing a solution of **1**·Et_3N in CH_2Cl_2 through a 5 g column of Amberlyst-15 (prewashed by soaking with EtOH and CH_2Cl_2) and eluting the column with 10:1 CH_2Cl_2/MeOH (step l, Figure 1). Pure **1** was obtained by crystallization from 1:1 $CHCl_3$/MeOH (step m, Figure 1). Application of this procedure to 1.8 g of XRI2009 and 2.1 g of XRI2132 afforded 12.8 and 8.4 mg, respectively.

(±)-Laetirobin (1): yellow needles (1:1 $CHCl_3$/MeOH), mp 235−238 °C (corrected against camphor at 179−180 °C); $[\alpha]^{20}_D$ 0.04 ± 0.01 (*c*

1.2, $CHCl_3$); UV−vis (DMSO) λ_{max} (log ϵ) 430 (5.06), 472 (5.06), 487 (5.15), 499 (5.16), 516 (5.15); IR (thin film) ν_{max} 2930 (broad), 1644, 1462, 1391, 1370, 1331, 1285, 1256, 1136, 1044 (weak), 988 (weak), 952 (w), 881 (weak), 797 (weak), 734 (weak) cm^{-1}; ^1H NMR (500 MHz, $CDCl_3$) δ 12.45 (s, OH, 2H), 12.44 (s, OH, 1H), 12.37 (s, OH, 1H), 7.92 (s, 1H), 7.91 (s, 1H), 7.90 (s, 1H), 7.68 (s, 1H), 7.00 (sm 1H), 6.96 (s, 1H), 6.96 (s, 2H), 6.57 (s, 1H), 6.48 (s, 1H), 6.47 (s, 1H), 6.47 (s, 1H), 4.47 (t, J = 5.5 Hz, 1H), 2.76 (m, 1H), 2.69 (m, 1H), 2.66 (s, 3H), 2.65 (s, 6H), 2.36 (m, 1H), 2.35 (s, 3H), 2.32 (m, 1H); ^{13}C NMR (100 MHz, $CDCl_3$) δ 204.2, 204.2, 204.1, 204.0, 161.5, 161.5, 161.4, 161.3, 159.8, 159.7, 159.7, 159.6, 158.7, 158.2, 157.3, 153.7, 144.7, 123.9, 123.9, 123.6, 123.3, 121.2, 120.8, 120.7, 119.5, 117.4, 117.2, 117.2, 115.9, 106.0, 105.6, 104.4, 100.4, 100.1, 100.1, 100.0, 43.5, 34.7, 31.3, 27.1, 27.1, 27.1, 26.9, 25.5; HREIMS *m/z* 752.1882 (calcd for $C_{44}H_{32}O_{12}$, 752.1894).

Acknowledgment. We thank the Ministry of Education of Singapore for funding (AcRF Tier-2 Grant T206B1112) and the National University of Singapore for a Graduate Scholarship (to O.S.).

Supporting Information Available: ^1H, ^{13}C, and selected 2D NMR spectra of (±)-laetirobin (**1**) are available free of charge via the Internet at http://pubs.acs.org.

References and Notes

(1) (a) Koehn, F. E.; Carter, G. T. *Nat. Rev. Drug Discovery* **2004**, *4*, 206–220. (b) Butler, M. S. *Nat. Prod. Rep.* **2008**, *25*, 475–516. (c) Butler, M. S.; Newman, D. J. *Prog. Drug. Res.* **2008**, *65*, 3–44. (d) Gordaliza, M. *Clin. Transl. Oncol.* **2007**, *9*, 767–776. (e) Kingston, D. G.; Newman, D. J. *Curr. Opin. Drug. Discovery Dev.* **2005**, *8*, 207–227. (f) Jones, W. P.; Chin, Y. W.; Kinghorn, A. D. *Curr. Drug Targets* **2006**, *7*, 247–264.

(2) (a) Adrian, T. E. *Curr. Pharm. Des.* **2007**, *13*, 3417–3426. (b) Newman, D. J.; Cragg, G. M. *J. Nat. Prod.* **2007**, *70*, 461–477. (c) Collins, I.; Workman, P. *Nat. Chem. Biol.* **2006**, *2*, 689–700.

(3) (a) Ryan, R. P.; Germaine, K.; Franks, A.; Ryan, D. J.; Dowling, D. N. *FEMS Microbiol. Lett.* **2008**, *278*, 1–9. (b) Zhang, H. W.; Song, Y. C.; Tan, R. X. *Nat. Prod. Rep.* **2006**, *23*, 753–771. (c) Gill, M.; Steglich, W. *Fortschr. Chem. Org. Naturst.* **1987**, *51*, 1–317.

(4) Steinkellner, S.; Lendzemo, V.; Langer, I.; Schweiger, P.; Khaosaad, T.; Toussaint, J. P.; Vierheilig, H. *Molecules* **2007**, *5*, 1290–1306.

(5) For natural products obtained from *L. sulphureus*, see: (a) Davoli, P.; Mucci, A.; Schenetti, L.; Weber, R. W. *Phytochemistry* **2005**, *66*, 817–823. (b) León, F.; Quintana, J.; Rivera, A.; Estévez, F.; Bermejo, J. *J. Nat. Prod.* **2004**, *67*, 2008–2011. (c) Yoshikawa, K.; Bando, S.; Arihara, S.; Matsumura, E. *Chem. Pharm. Bull.* **2001**, *49*, 327–329. The latter reference is particularly relevant, as it identifies a monobenzofuran that exhibited cytotoxicity against Kato III cells.

(6) Cochran, K. W. *McIlvainea* **2000**, *14*, 34–40.

(7) (a) Rodríguez, A. D.; Lear, M. J.; La Clair, J. J. *J. Am. Chem. Soc.* **2008**, *130*, 7256–7258. (b) Hughes, C. C.; MacMillan, J. B.; Gaudêncio, S. P.; Fenical, W.; La Clair, J. J. *Angew. Chem., Int. Ed.* **2009**, *48*, 728–732.

(8) Alexander, M. D.; Burkart, M. D.; Leonard, M. S.; Portonovo, P.; Liang, B.; Ding, X.; Joullie, M. M.; Gulledge, B. M.; Aggen, J. B.; Chamberlin, A. R.; Sandler, J.; Fenical, W.; Cui, J.; Gharpure, S. J.; Polosukhin, A.; Zhang, H. R.; Evans, P. A.; Richardson, A. D.; Harper, M. K.; Ireland, C. M.; Vong, B. G.; Brady, T. P.; Theodorakis, E. A.; La Clair, J. J. *ChemBioChem* **2006**, *7*, 409–416.

(9) Schorl, C.; Sedivy, J. M. *Methods* **2007**, *41*, 143–150.

(10) Jackman, J.; O'Connor, P. M. *Curr. Protoc. Cell. Biol.* **2001**, *8.3*, 1–20.

(11) Although sufficient for guiding the isolation of **1**, this process failed to provide sufficient quantities of probe **3** for characterization by NMR analysis. As probe **3** was unnecessary for this study, we did not prepare samples for structural assignment. Efforts are ongoing to apply IAF-labeling methods to develop active probes for molecular and cellular studies as well as to define the structure−activity relationships of **1**. These efforts will be reported in due course.

(12) The 1024 *m/z* peak identified from probe **3** during reverse-affinity purification was used to guide preparative isolation of compound **1** (steps h−m, Figure 1). For procedures for DCVC, see: Pedersen, D. S.; Rosenbohm, C. *Synthesis* **2001**, *16*, 2431–2434.

(13) The use of H/C ratios to determine the applicability of NMR methods was first described by: Crews, P. US-Japan Conference on Marine Natural Products Chemistry (June 2007).

(14) Goel, A.; Dixit, M. *Synlett* **2004**, *11*, 1990–1994.

(15) (a) Wolf, D. E. *Methods Cell Biol.* **2007**, *81*, 63–91. (b) Jonker, A.; Geerts, W. J.; Chieco, P.; Moorman, A. F.; Lamers, W. H.; Van Noorden, C. J. *Histochem. J.* **1997**, *29*, 347–364.

(16) Lemieux, B.; Percival, M. D.; Falgueyret, J. P. *Anal. Biochem.* **2004**, *327*, 247–251.

(17) Bicamumpaka, C.; Page, M. *Int. J. Mol. Med.* **1998**, *2*, 161–165.

(18) Verderame, M.; Alcorta, D.; Egnor, M.; Smith, K.; Pollack, R. *Proc. Natl. Acad. Sci. U.S.A.* **1980**, *77*, 6624–6628.

(19) For recent perspectives on antimitotic agents, see: (a) Jackson, J. R.; Patrick, D. R.; Dar, M. M.; Huang, P. S. *Nat. Rev. Cancer* **2007**, *7*, 107–117. (b) Ruchaud, S.; Carmena, M.; Earnshaw, W. C. *Nat. Rev. Mol. Cell Biol.* **2007**, *8*, 798–812. (c) Ivachtchenko, A. V.; Kiselyov, A. S.; Tkachenko, S. E.; Ivanenkov, Y. A.; Balakin, K. V. *Curr. Cancer Drug Targets* **2007**, *7*, 766–784. (d) Weaver, B. A. A.; Cleveland, D. W. *Cancer Cell.* **2005**, *8*, 7–12.

(20) Benzofuran-containing natural products have been observed in fungi; see: (a) Manniche, S.; Sprogøe, K.; Dalsgaard, P. W.; Christophersen, C.; Larsen, T. O. *J. Nat. Prod.* **2004**, *67*, 2111. However, they are more commonly obtained from plant extracts. For recent examples describing the isolation of benzofuran-containing natural products from plants, see: (b) Shen, H.; Hou, A. *J. Nat. Prod. Res.* **2008**, *22*, 1451–1456. (c) Chen, T. H.; Liau, B. C.; Wang, S. Y.; Jong, T. T. *Planta Med.* **2008**, *74*, 1806–1811. (d) Ross, S. A.; Rodríguez-Guzmán, R.; Radwan, M. M.; Jacob, M.; Ding, Y.; Li, X. C.; Ferreira, D.; Manly, S. P. *J. Nat. Prod.* **2008**, *71*, 1764–1767.

(21) We have recently completed a total synthesis of (±)-laetirobin (**1**) that suggests that the biosynthesis arises through a homodimeric Diels−Alder cycloaddition; see: Simon, O.; Reux, B., La Clair, J. J.; Lear, M. J. *Chem Asian J.*, in review.

(22) Sapan, C. V.; Lundblad, R. L.; Price, N. C. *Biotechnol. Appl. Biochem.* **1999**, *29*, 99–108.

NP9002838